University Center of Barika
The 1st National Conference on Electrical Engineering, Renewable Energy, and Artificial Intelligence"NCEERA'26"
January 25, 2026

Performance Analysis of a PV-Powered Water Pumping System Based on P&O MPPT and Induction Motor Drive.

1st Lahlah Salah
:LEB Research Laboratory, Electrical Engineering Department, University of Mostefa Ben Boulaïd Batna 2, Algeria
salahlahlah1970@gmail.com

2st Lakhdar Neceredine
:LEB Research Laboratory, Electrical Engineering Department, University of Mostefa Ben Boulaïd Batna 2, Algeria
n.lakhdar@univ-batna2.dz

3st Choug Noreddine
Electrical Engineering Laboratory (LGE), Electrical Engineering Department, Faculty of Technology. University of M'Sila, University Pole, Road Bordj Bou Arreridj M'sila 28000, Algeria.
choug.noreddine@univ-msila.dz

4st Dilmi Smail
LASS, Laboratory of Analysis of Signals and Systems, Electrical Engineering Department, Faculty of Technology. University of M'Sila, University Pole, Road Bordj Bou Arreridj M'sila 28000, Algeria.
smail.dilmi@univ-msila.dz

***Abstract*—**
This paper presents the modeling and simulation of a standalone photovoltaic (PV) water pumping system composed of a PV generator, a DC–DC boost converter, a three-phase inverter, an induction motor, and a centrifugal pump. A Perturb and Observe (P&O) maximum power point tracking (MPPT) algorithm is used to control the duty cycle of the boost converter in order to ensure maximum power extraction under variable irradiance and temperature conditions. The complete system is implemented in MATLAB/Simulink using a 2.5-kW PV array based on BP SX-150S modules. Simulation results show that the proposed MPPT maintains the PV array operation close to the maximum power point with fast convergence and limited steady-state oscillations. The motor speed, inverter currents, and pump operation remain stable despite environmental variations, confirming the suitability of the proposed system for standalone water pumping applications.

Keywords— Photovoltaic Generator , Static Converter ,Asynchronous Motor ,Centrifugal Pump ,PWM Control, MPPT (Maximum Power Point Tracking)

I. Introduction

Water resources are vital for human needs, public health, food production, energy supply, and socio-economic development. However, water scarcity remains a serious global issue, with nearly two billion people in more than forty countries affected and about 1.1 billion lacking access to safe drinking water [1]. In this context, photovoltaic (PV) energy has become an attractive and sustainable solution for water pumping, especially in remote and isolated areas. Algeria has strong solar potential due to its high year-round irradiance, making solar-powered pumping systems a promising alternative to conventional energy sources, particularly in rural and desert regions [2–6].

A typical PV water pumping system includes a PV generator, power electronic converters (a DC–DC boost converter and a three-phase inverter), an electric motor, and a centrifugal pump [3]–[7]. Induction motors are commonly used because of their robustness, low cost, and low maintenance, while the centrifugal pump load depends on the motor speed, enabling control of water flow and head.

Since PV output is highly dependent on irradiance and temperature, the operating point rarely coincides with the maximum power point. Therefore, maximum power point tracking (MPPT) techniques are widely used to ensure optimal energy extraction under changing conditions [1–5].

This paper presents the modeling and simulation of a 2.5-kW standalone PV water pumping system using a Perturb and Observe (P&O) MPPT algorithm. The PV generator, converters, induction motor, and centrifugal pump are modeled in MATLAB/Simulink to evaluate system performance under variable irradiance and temperature.

The paper is organized as follows: Section II describes the system configuration and models, Section III presents the simulation results, and Section IV concludes the paper and outlines future work.

II. Bloc diagram of a photovoltaic pumping system

The present work aims to investigate a photovoltaic (PV) water pumping system operating at its maximum power point. To achieve this, the PV system must include a power adaptation stage associated with a Maximum Power Point Tracking (MPPT) algorithm [1-4].
In this study, the widely used Perturb and Observe (P&O) algorithm was implemented to ensure optimal power extraction from the PV array while providing the ability to regulate the water flow. The pumping system under consideration consists of a pumping chain driven by a three-phase asynchronous motor.

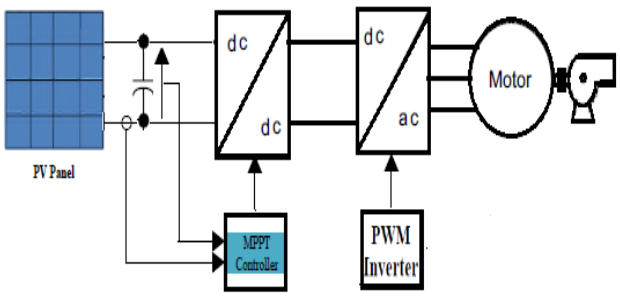

Fig. 1. Illustrates the overall PV-based driver circuit for water pumping, highlighting the integration of the PV array, MPPT controller, and motor drive.

A. Solar cell model

The electrical behavior of a photovoltaic (PV) cell has been extensively studied over the past four decades. A general mathematical description of the current-voltage (I–

V) characteristics of a PV cell is widely used for modeling and analysis. The equivalent circuit of a typical PV cell consists of a photocurrent source, a diode, and a series resistor representing the internal resistance to current flow, as shown in Fig. 2. The voltage-current characteristic equation of the solar cell can be expressed as [8]:

$$I_{pv} = I_{sc} - I_0\left[e^{\frac{V_{PV}+R_S I_{PV}}{V_t}} - 1\right] \quad (1)$$

where the thermal voltage V_t is defined as:

$$V_t = \frac{n*K*T}{q} \quad (2)$$

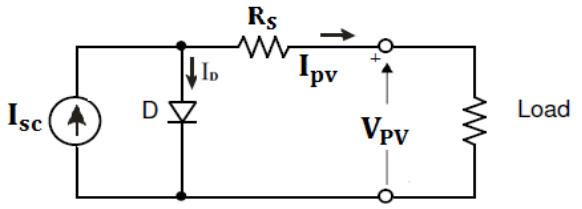

Fig. 2. Simplified equivalent circuit of a photovoltaic cell.

The PV cell output current is determined by the interplay of the photocurrent, diode current, and series resistance. The main variables are defined as follows:

- I_{sc} : photocurrent (A) .
- I_D : diode current (A).
- I_{PV} : cell output current (A) .
- V_{PV} : cell output voltage (V).
- R_S : series resistance of the cell (Ω).

with:

- I_0 cell saturation (dark) current (A).
- n=1.6 : ideality factor
- k :$1.381x10^{-23}J/K$: Boltzmann constant
- T : cell operating temperature (K)
- $q = 1.602x10^{-19}C$) electron charge

The photocurrent depends primarily on solar irradiation and the cell temperature:

$$I_{sc} = G * I_{sc_{Tréf}} * [1 + \alpha(T - T_{réf})] \quad (3)$$

Where

- $I_{sc\_Tréf}$: Short-circuit current at 25°C and 1 kW/m².
- α =0.65*$10^{-3:}$ temperature coefficient of the short-circuit current.
- $T_{réf}$: Reference temperature (K).
- G: solar insolation (kW/m²)

The saturation current varies with cell temperature as follows:

$$I_{0\_Tref} = \frac{I_{sc\_Tréf}}{e^{V_{oc\_Tref}/V_{t\_Tref}} - 1} \quad (4)$$

$$I_{0\_T} = I_{0\_Tréf} * \left(\frac{T}{T_{réf}}\right)^3 * e^{\beta\left(\frac{1}{T_{réf}} - \frac{1}{T}\right)} \quad (5)$$

$$\beta = \frac{E_g * q * K}{n} \quad (6)$$

where:

- $I_{0\_Tréf}$: reverse saturation current at reference temperature and radiation
- $E_g = 1.2eV$: semiconductor band-gap energy.

These equations provide a comprehensive description of the PV cell behavior under varying solar irradiation and temperature conditions, forming the basis for accurate modeling of photovoltaic systems.

B. Solar module and array model

A single photovoltaic (PV) cell typically generates less than $2\,W$ at an operating voltage of approximately$0.5\,V$. Therefore, multiple PV cells must be electrically connected in series–parallel configurations to form a PV module capable of delivering higher voltage and power levels.

A PV array consists of several PV modules interconnected in series and parallel arrangements to obtain the required output current and voltage. The equivalent electrical circuit of a solar module composed of N_P parallel branches and N_S series-connected cells is considered in this study.

Based on this configuration, the terminal current–voltage relationship of the PV array can be expressed as follows [8]

$$I_{pv} = N_P I_{sc} - N_P I_0 \left(e^{\left(q\frac{\left(\frac{V_{PV}}{N_S} + \frac{R_S I_{pv}}{N_P}\right)}{nKT} \right)} - 1 \right) \quad (7)$$

- R_s : equivalent series resistance of the array (Ω)
- Isc : short-circuit current of a single cell (A)
- I0 : reverse saturation current (A)
- n : diode ideality factor
- k : Boltzmann constant
- T : cell temperature (K)
- q : electron charge.

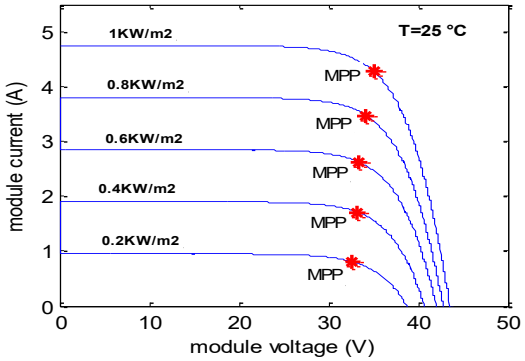

Fig. 3. PV current voltage with different G.

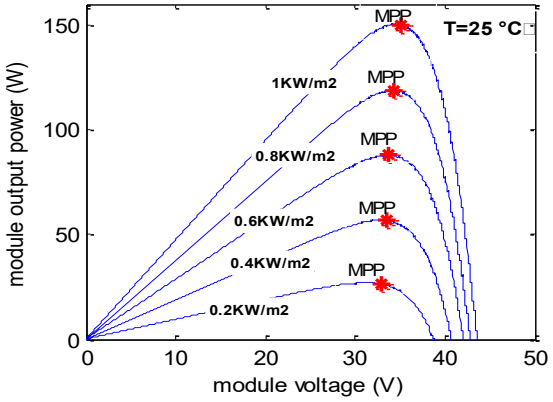

Fig. 4. Power voltagel with different G.

Figures 3 and 4 illustrate the I–V and P–V characteristics of the PV array under different temperatures, showing the decrease in open-circuit voltage and maximum power as temperature increases. Figures 5 and 6 shows the same characteristics under varying irradiance, confirming that the output current and power are proportional to solar radiation.

These curves justify the need for MPPT to continuously track the maximum power point.

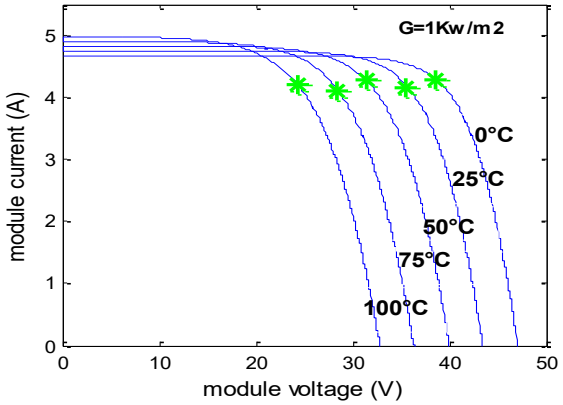

Fig. 5. PV current_voltage with different T.

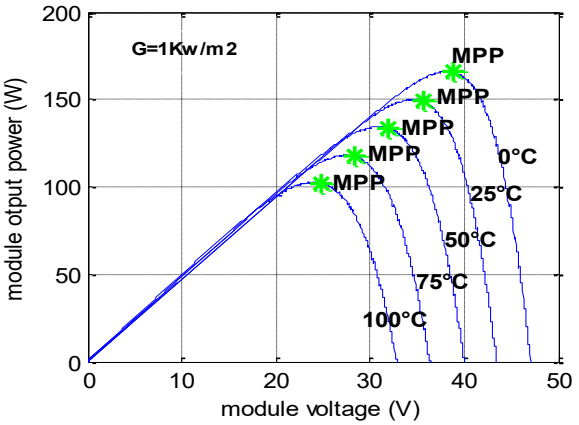

Fig. 6. Power voltagel with different T.

C. DC–DC BOOST CONVERTER

The Boost converter shown in Fig. 7 is used as the DC–DC interface in this study. It is a step-up converter that produces an output voltage higher than the PV voltage (Vout > VPV). It is composed of an inductor, a controlled switch, a diode, and an output capacitor. Energy is stored in the inductor when the switch is on and transferred to the load when the switch is off. The converter is designed to operate in continuous conduction mode (CCM), where the inductor current never reaches zero. This mode is well suited for photovoltaic systems because it reduces current ripple, improves efficiency, and ensures stable and smooth interaction with the MPPT controller under changing irradiance conditions. [9–12].

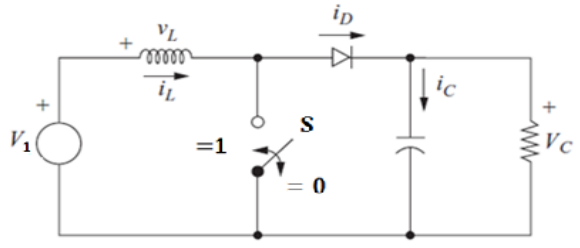

Fig. 7. Electrical schematic of the DC–DC Boost converter.

$$\frac{dI_L}{dt} = \left(\frac{1}{L}\right)[V_1 - (1 - S)V_C] \quad (8)$$

$$\frac{dV_C}{dt} = \left(\frac{1}{C}\right)\left[(1 - S)I_L - \frac{V_C}{R}\right] \quad (9)$$

III. Perturb and observe (P&O) method

The Perturb and Observe (P&O) method is a widely used MPPT technique for photovoltaic systems due to its simple structure and the use of only two measured variables, the PV voltage V_{PV} and current I_{PV}. The algorithm perturbs the operating voltage and observes the resulting change in output power to determine the direction toward the maximum power point.

By comparing successive power values, the algorithm decides whether to keep or reverse the perturbation direction, allowing continuous convergence to the maximum power point even under changing irradiance and temperature conditions. The implementation of the P&O algorithm is illustrated in Fig. 8 [13–16].

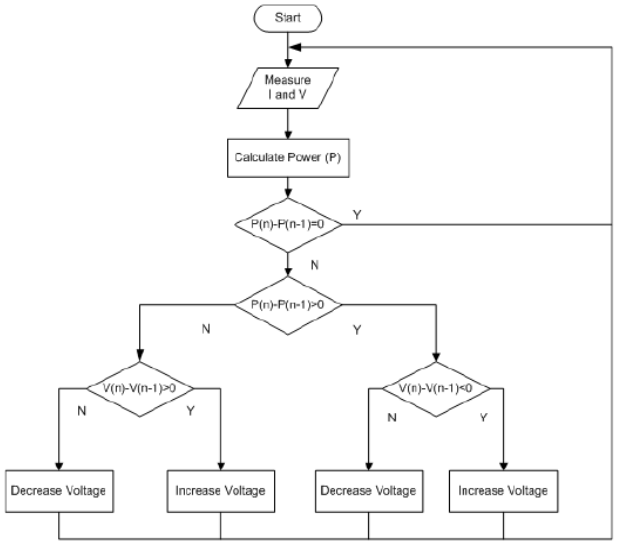

Fig. 8. Flowchart of the Perturb and Observe (P&O) MPPT algorithm.

At each sampling instant, the instantaneous PV power is calculated as:

$$P_{PV}.(t) = V_{PV}(t) \cdot I_{PV}(t) \quad (10)$$

The computed power is then compared with the previous value $P_{PV}(t-1)$

- If $P_{PV}.(t) > P_{PV}.(t-1)$), the operating point moves toward the maximum power point, and the perturbation direction is maintained.
- If $P_{PV}.(t) < P_{PV}.(t-1)$), the operating point moves away from the maximum power point, and the perturbation direction is reversed.

This iterative process ensures convergence toward the MPP and continuous tracking under changing environmental conditions.

In this study, the P&O algorithm directly controls the duty cycle D of the DC–DC Boost converter. The duty cycle is updated according to the following rule:

$$D(t) = D(t-1) \pm \Delta D \quad (11)$$

where ΔD represents the perturbation step size.

The decision logic depends on the sign of both the power variation and the duty cycle variation, as illustrated in the flowchart of Fig. 8.

IV. Modeling of the three-phase inverter

An inverter converts DC voltage into a symmetrical AC voltage with controlled amplitude and frequency. This can be achieved by adjusting the DC input or by using suitable control methods. Among these, Pulse Width Modulation (PWM) is the most commonly used technique because of its simplicity, high efficiency, and good harmonic performance. PWM enables accurate control of the inverter output by modulating the switching signals of the power devices [9].

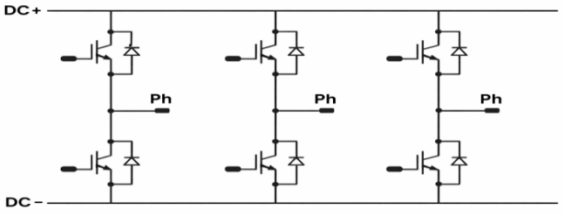

Fig. 9. Three-phase voltage source inverter..

For a three-phase voltage source inverter, the phase voltages can be expressed as follows

$$\begin{bmatrix} V_{an} \\ V_{bn} \\ V_{cn} \end{bmatrix} = \frac{U_0}{3} \begin{bmatrix} 2 & -1 & -1 \\ -1 & 2 & -1 \\ -1 & -1 & 2 \end{bmatrix} \begin{bmatrix} f_{c1} \\ f_{c2} \\ f_{c3} \end{bmatrix} \quad (12)$$

Where: U_0 DC bus voltagef_{c1} ; f_{c2} ; f_{c3} switching functions of the inverter legs V_{an} V_{bn} V_{cn} phase voltages with respect to the neutral point.

$$I_S = I_a f_{c1} + I_b f_{c2} + I_c f_{c3} = \sqrt{(I_{sd})^2 + \left(I_{sq}\right)^2} \quad (13)$$

V. Modeling of the asynchronous machine

The the asynchronous machine model, represented in the d-q Park reference frame, is described by the following equations [16-17].

$$\begin{cases} V_{sd} = R_s I_{sd} + \frac{d\varphi_{sd}}{dt} - \omega_s \varphi_{sq} \\ V_{sq} = R_s I_{sq} + \frac{d\varphi_{sq}}{dt} + \omega_s \varphi_{sd} \\ 0 = R_r I_{rd} + \frac{d\varphi_{rd}}{dt} - \omega_r \varphi_{rq} \\ 0 = R_r I_{rq} + \frac{d\varphi_{rq}}{dt} + \omega_r \varphi_{rd} \end{cases} \quad (14)$$

The stator and rotor flux can be expressed as:

$$\begin{cases} \varphi_{sd} = L_s I_{sd} + M I_{rd} \\ \varphi_{sq} = L_s I_{sq} + M I_{rq} \\ \varphi_{rd} = L_r I_{rd} + M I_{sd} \\ \varphi_{rq} = L_r I_{rq} + M I_{sq} \end{cases} \quad (15)$$

Where

s, r are stator and rotor subscripts,V_{sd}, V_{sq}, V_{rd},and $V_{rq}$are respectively the direct and quadrate stator and rotor voltages,$I_{sd}, I_{sq}, I_{rd}$and $I_{rq}$are respectively the direct and quadrate stator and rotor currents ,$\varphi_{sd}, \varphi_{sq}, \varphi_{rd}$,and φ_{rq} are respectively the direct and quadrate stator and rotor fluxes,L_s, L_r, M stator and rotor per phase winding and magnetizing inductances,$P$is the pair pole number,R_s and R_r are the stator and rotor phase resistances respectively, ω_s, ω_r are respectively the synchronous angular speed of the the asynchronous machine and the angular speed of the rotor.

The electromagnetic torque is expressed in terms of currents and fluxes by:

$$T_{em} = p \frac{M}{L_s} (I_{rq} \varphi_{sd} - I_{rd} \varphi_{sq}) \quad (16)$$

VI. Modeling of the centrifugal pump

The hydraulic behavior of a centrifugal pump is commonly described by its head–flow (H–Q) characteristic. In this study, the pump characteristic is approximated using the Pleĭder–Peterman model, which provides an accurate analytical representation of centrifugal pump performance.

The total manometric head (TMH) of the pump can be expressed as:

$$\mathrm{TMH} = C_1 \Omega^2 - C_2 \Omega Q - C_3 Q^2 \quad (17)$$

Where:

C_1, C_2, C_3 : pump characteristic constants

Ω : rotational speed of the pump (rpm)

Q : water flow rate (m^3/h)

The centrifugal pump applies a resistive torque to the motor that is proportional to the square of its rotational speed and is given by:

$$C_r = K_r * \Omega^2 \quad (18)$$

Ω **:** angular speed of the asynchronous motor (rad/s)

K_r **:** proportionality coefficient [Nm/(rad.s^{-1})^2]

The coefficient K_r is calculated from the nominal operating conditions as:

$$K_r = \frac{P_n}{\Omega_n^3} \quad (19)$$

p_n **:** nominal power of the asynchronous motor (W)

Ω_n : nominal angular speed of the motor (rad/s)

VI. Simulation results and discussions

This section presents the MATLAB/Simulink simulation results of the PV water pumping system under variable irradiance and temperature. The system dynamics and the performance of the P&O MPPT algorithm are analyzed through electrical, mechanical, and hydraulic variables, showing stable operation and effective power tracking.

The system components, including the PV generator, power electronics, motor, and pump, are accurately modeled to ensure realistic performance evaluation. The PV generator is based on the BP SX 150S module, whose main characteristics under standard test conditions are given in Table I [1].

TABLE I. *ELECTRICAL CHARACTERISTICS OF THE BP SX 150S PV MODULE*

Parameter	Symbol	Value
Maximum power	P_{max}	150 W
Voltage at maximum power	V_{mp}	34.5 V
Current at maximum power	I_{mp}	4.35 A
Open-circuit voltage	V_{OC}	43.5 V
Short-circuit current	I_{SC}	4.75 A
Temperature coefficient of ISC	$\propto_{ISC}$	0.065 %/°C
Temperature coefficient of VOC	$\propto_{Voc}$	−160 mV/°C
Temperature coefficient of power	$\propto_P$	−0.5 %/°C
Nominal operating cell temperature	NOCT	47 ± 2 °C

The DC link capacitor used to smooth the DC voltage is defined as: $C_{DC} = 10 * 10^{-6} F$.

The motor parameters used in the simulation are summarized in Table II.

TABLE II. *ASYNCHRONOUS MOTOR PARAMETERS*

Parameter	Symbol	Value
Nominal power	P_n	2.2 kW
Nominal frequency	f_n	50 Hz
Line-to-line voltage	V_{LL}	208 V
Number of poles	P	4
Stator resistance	R_s	0.6 Ω
Rotor resistance	R_r	0.4 Ω
Stator inductance	L_s	61 mH
Rotor inductance	L_r	61 mH
Mutual inductance	M	59 mH
Rotor inertia	J	0.0175 kg·m²
Viscous friction coefficient	F	0.00187 N·m·s/rad

The centrifugal pump model is defined by the Pleĭder–Peterman coefficients as follows:

$$\begin{cases} C_1 = 6.6587 * 10^{-6} \\ C_2 = 6.8965 * 10^{-5} \\ C_3 = -0.02 \end{cases}$$

These parameters characterize the hydraulic behavior of the

pump and are used to compute the head–flow relationship and load torque.

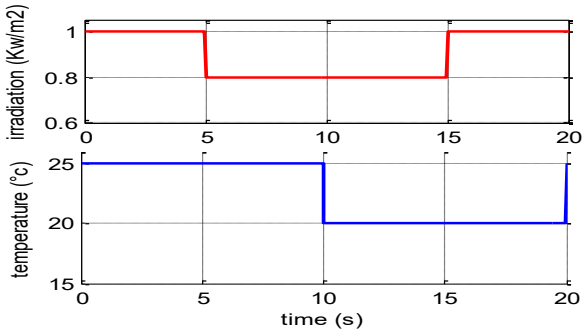

Fig. 10. Sollaire irradiation and temperature

Figure 10 presents the solar irradiance and temperature profiles used to test the MPPT robustness, while Fig. 11 shows the boost converter duty cycle, which adapts smoothly to irradiance changes, indicating stable MPPT operation.

Figures 12 and 13 illustrate the PV output power and voltage, showing effective tracking of the maximum power point with small oscillations inherent to the P&O method. Figure 14 presents the PV current variation, which follows the irradiance profile, confirming proper energy extraction.

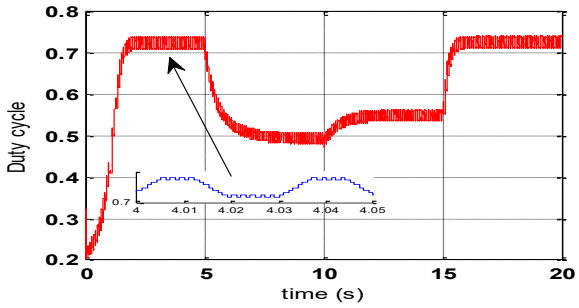

Fig. 11. Duty cycle.

Fig 15. This figure presents a balanced and sinusoidal inverter phase voltage, demonstrating correct PWM operation.and Fig 16. illustrates the inverter phase current, synchronized with the voltage, indicating proper motor operation.Fig 17. shows the motor speed response, which stabilizes according to the available photovoltaic power, ensuring reliable pumping operation

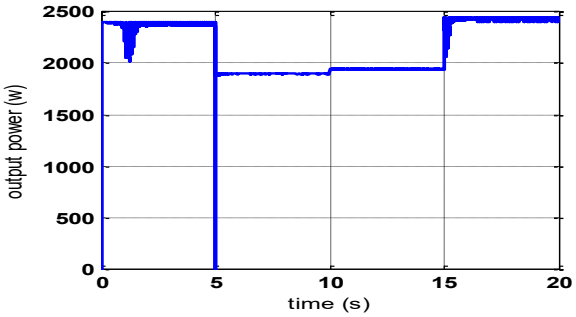

Fig. 12. output power

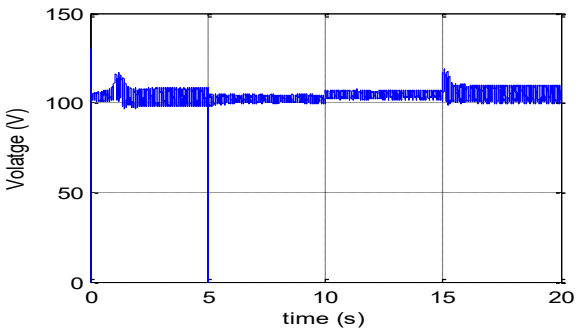

Fig. 13. Voltage GPV.

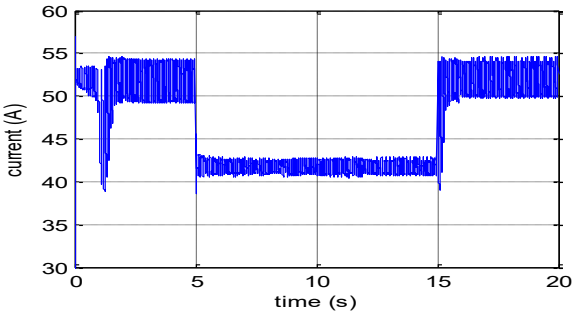

Fig. 14. Current GPV.

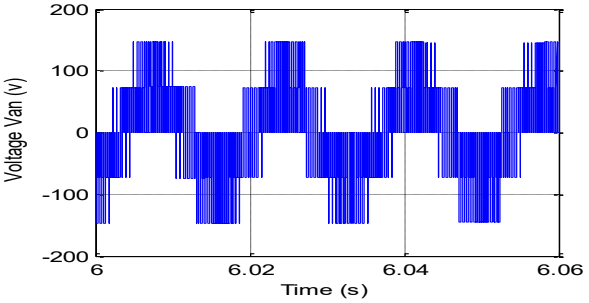

Fig. 15. Voltage Van.

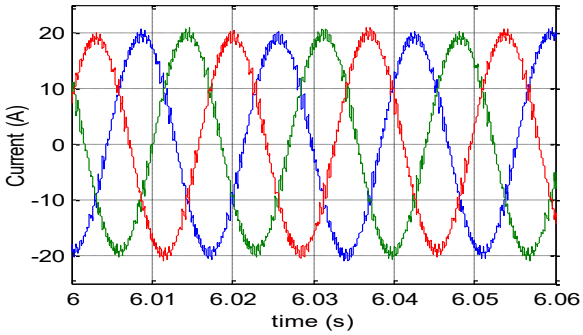

Fig. 16. current Ian.

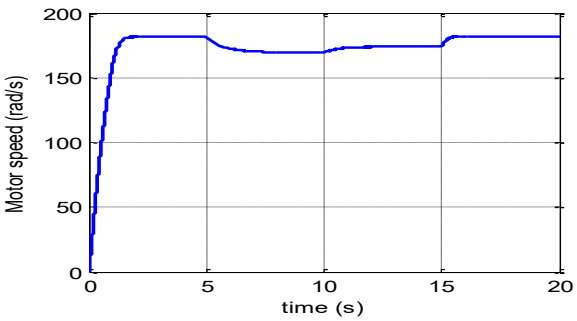

Fig. 17. Motor speed

VII. Conclusion

This paper presented the modeling and simulation of a standalone PV water pumping system composed of a PV generator, a DC–DC boost converter, an MPPT controller, a three-phase inverter, an induction motor, and a centrifugal pump. The P&O MPPT algorithm ensured effective maximum power tracking under varying irradiance and temperature. Simulation results demonstrated stable DC voltage, balanced inverter outputs, and smooth motor operation, confirming the reliability of the proposed system for standalone pumping applications. Future work will focus on advanced MPPT methods, energy storage integration, and experimental validation.

REFERENCES

[1] Akiro Oi : Design and simulation of photovoltaic water pumping system,A thesis presented to the faculty of california polytechnic state university san luis obispo,september 2005.

[2] N. Choug : Commande des Entrainements Electriques des Systèmes de Chaîne de Conversion d'Energie Renouvelable, PHD Thesis, University of Batna 02, 2021.

[3] A.Bouden, M.Marir Benabbas : Modélisation de système de pompage photovoltaïque optimisé, conférence Internationale des Energies Renouvelables (CIER'13) Sousse, Tunisie-2013

[4] M. Eltawil, Z. Zhao: MPPT techniques for photovoltaic applications, Renewable and Sustainable Energy Reviews. Vol. 25, pp. 793-813. 2013.

[5] R. Teodorescu, M. Liserre, P. Rodriguez: Grid Converters for Photovoltaic and Wind Power Systems, West Sussex UK Wiley, 2011

[6] Mohd Saifuzam Jamri and Tan Chee Wei: Modeling and Control of a Photovoltaic Energy System Using the State-Space Averaging Technique, American Journal of Applied Sciences 7(5): pp. 682-691,2010

[7] [7] M.N.Mansouri ; N.Ghanmi et M.F.Mimouni : Commande et analyse des performances d'une station de pompage photovoltaïque fonctionnant en régime optimale, Revue des Energies Renouvelables Vol.11 N°1, pp.1-17 (2008) .

[8] Huan-Liang Tsai , Ci-Sing Tu , and Yi-Jie Su Member ,IAENG : Development of Generalized photovoltaic Model Using matlab/simulink , Proceeding of the World Congress on Engineering and Computer Science San Francisco, USA, October 22-24,2008,

[9] N.Nisso, D.Raidandi, N. Djongyang and F.D.Menga : Modeling and analysis of boost converter in small-signal applied to the wind energy coversion system using matlab/simulink, Revue des Energies Renevelables Vol.21 N^0 4 , pp 635-649. 2018

[10] M. Taghvaee, M. Radzi, S. Moosavain, H. Hashim, M. Hamiruce: A current and future study on non-isolated dc-dc converters for photovoltaic applications, Renewable and Sustainable Energy Reviews. Vol 17, pp. 216- 227. 2013.

[11] G. Dileep, S. Singh: Selection of non-isolated DC-DC converters for solar photovoltaic system, Renewable and Sustainable Energy Reviews. Vol. 76, pp. 1230-1247. 2017.

[12] [12] M.F. Iacchetti, G.D. Marques, R. Perini: A scheme for the Power Control in a DFIG Connected to a DC Bus via a Diode Rectifier, IEEE Transactions on Power Electronics, Vol. 30, Nº. 3, pp. 1286 – 1296. 2015,

[13] A. Gupta, Y. Chauhan, R. Kumar: A comparative investigation of maximum power point tracking methods for solar PV system, Solar Energy. Vol. 136, pp. 236- 253. 2016.

[14] P. Mohanty, G. Bhuvaneswari, R. Balasubramanian, N. Dhaliwal: MATLAB based modeling to study the performance of different MPPT techniques used for solar PV system under various operating conditions, Renewable and Sustainable Energy Reviews. Vol. 38, pp. 581-593. 2014.

[15] Ahmed M. Atallah, Almoataz Y. Abdelaziz, and Raihan S. Jumaah: Implementation of Perturb and Observe MPPT of PV System with Direct Control Method Using Buck and Buck boost Converters, Emerging Trends in Electrical, Electronics & Instrumentation Engineering, An international Journal (EEIEJ), Vol. 1, Nº. 1, February 2014

[16] N. Choug, S. Benaggoune, S. Belkacem, Hybrid Fuzzy Reference Signal Tracking Control of a Doubly Fed Induction Generator, IJE transactions A: Basics,vVol. 33, No. 4, pp. 567–574, Apr. 2020

[17] N. Choug, S. Belkacem, S. Benaggoune , Advanced Direct Torque Control: Employing Fuzzy Logic for Dynamic and Adaptive Regulation, Automatika, Vol 20, No. 3 , pp. 9289 - 9300, 2024.